JGP Journal of General Physiology

METHODS AND APPROACHES

Electrical recordings of the mitochondrial calcium uniporter in *Xenopus* oocytes

Chen-Wei Tsai[1] and Ming-Feng Tsai[1,2,3]

The mitochondrial calcium uniporter is a multisubunit Ca^{2+} channel that mediates mitochondrial Ca^{2+} uptake, a cellular process crucial for the regulation of oxidative phosphorylation, intracellular Ca^{2+} signaling, and apoptosis. In the last few years, genes encoding uniporter proteins have been identified, but a lack of efficient tools for electrophysiological recordings has hindered quantitative analysis required to determine functional mechanisms of this channel complex. Here, we redirected Ca^{2+}-conducting subunits (MCU and EMRE) of the human uniporter to the plasma membrane of *Xenopus* oocytes. Two-electrode voltage clamp reveals inwardly rectifying Ca^{2+} currents blocked by a potent inhibitor, Ru360 (half maximal inhibitory concentration, ~4 nM), with a divalent cation conductivity of $Ca^{2+} > Sr^{2+} > Ba^{2+}$, Mn^{2+}, and Mg^{2+}. Patch clamp recordings further reveal macroscopic and single-channel Ca^{2+} currents sensitive to Ru360. These electrical phenomena were abolished by mutations that perturb MCU-EMRE interactions or disrupt a Ca^{2+}-binding site in the pore. Altogether, this work establishes a robust method that enables deep mechanistic scrutiny of the uniporter using classical strategies in ion channel electrophysiology.

Introduction

The mitochondrial calcium uniporter (henceforth denoted the uniporter) is a Ca^{2+} channel that imports cytoplasmic Ca^{2+} through the inner mitochondrial membrane (IMM) into the mitochondrial matrix (Bernardi, 1999; Gunter et al., 2000; Kirichok et al., 2004). It regulates a wide range of physiological processes, including aerobic metabolism, intracellular Ca^{2+} signaling, and apoptotic cell death (Rizzuto et al., 2012; Kamer and Mootha, 2015). Dysfunction of this channel has been implicated in a multitude of cardiovascular and neuromuscular pathologies (Logan et al., 2014; Kwong et al., 2015; Luongo et al., 2015; Liu et al., 2016; Penna et al., 2018). Breakthroughs in the last few years have led to identification of uniporter genes (Baughman et al., 2011; De Stefani et al., 2011; Mallilankaraman et al., 2012; Sancak et al., 2013), revealing that this channel is a protein complex containing at least four subunits: MCU, EMRE, MICU1, and MICU2 (Fig. 1). It has been shown that MCU pentamerizes to form a Ca^{2+} pathway traversing the IMM (Oxenoid et al., 2016), and that EMRE opens the MCU pore by associating with MCU via transmembrane (TM)–helix interactions (Sancak et al., 2013; Tsai et al., 2016). MICU1 and MICU2 are regulatory subunits in the intermembrane space (IMS), functioning to shut the uniporter when free Ca^{2+} in the IMS (and hence the cytoplasm) falls below 1 μM (Mallilankaraman et al., 2012; Csordás et al., 2013; Tsai et al., 2016; Kamer et al., 2017).

Fundamental properties of ion channels, including ion permeation and gating, are traditionally studied using electrophysiological recordings under voltage-clamp conditions. However, applying this approach to the uniporter has been difficult because of its limited electrical accessibility as an organellar channel. The Clapham laboratory developed a mitoplast patch clamp technique to record uniporter currents in mitochondria (Kirichok et al., 2004), but this method is of the "heroic" variety, not suitable for routine, multiply replicated experiments necessary for in-depth quantitative analysis. Recently, there have been reports of single-channel uniporter recordings in reconstituted planar bilayers (De Stefani et al., 2011; Patron et al., 2014; Wu et al., 2018). However, the quality of proteins used in these studies was unclear, and the observed electrical properties are vastly different from data obtained with the mitoplast patch clamp (Kirichok et al., 2004).

Here, we establish an efficient method using a two-electrode voltage clamp (TEVC) and patch clamp to record electrical activity of the human uniporter targeted to the plasma membrane of *Xenopus laevis* oocytes. We show that the uniporter mediates inwardly rectifying Ca^{2+} currents, inhibited by Mn^{2+} and blocked by a potent and specific inhibitor, Ru360 (Ying et al., 1991; Matlib et al., 1998), with a divalent cation conductivity of $Ca^{2+} > Sr^{2+}$ and Ba^{2+}, Mn^{2+}, and Mg^{2+} currents undetectable. These electrical

[1]Department of Biochemistry, Brandeis University, Waltham, MA; [2]Department of Physiology and Biophysics, University of Colorado Anschutz Medical Campus, Aurora, CO; [3]Howard Hughes Medical Institute, Chevy Chase, MD.

Correspondence to Ming-Feng Tsai: mftsai@brandeis.edu.

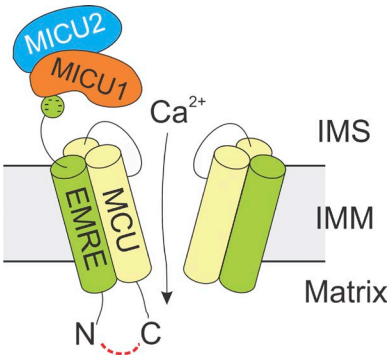

Figure 1. **Subunit assembly in the uniporter complex.** The red dashed line indicates how MCU and EMRE are fused to produce the hME tandem construct.

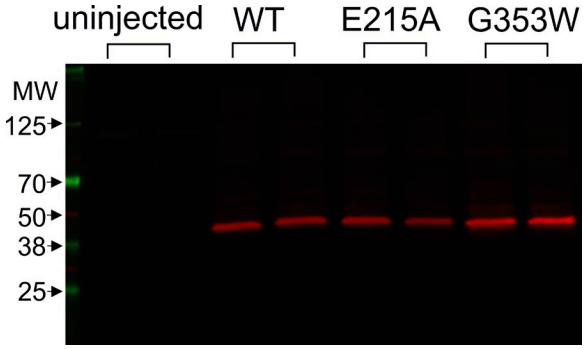

Figure 2. **Expression of hME in *Xenopus* oocytes.** The Western blot image shows expression of WT hME and two nonfunctional mutants. Each lane represents an independent repeat. Oocytes were injected with 12 ng cRNA and harvested after 3–4 d of incubation. 25 oocytes were used for each membrane preparation. MW, molecular weight.

phenomena are strictly absent in nonfunctional mutants or uninjected controls. With this new tool, it is now possible to perform iterative electrophysiological analysis to determine fundamental molecular mechanisms of the uniporter.

Materials and methods

Molecular biology

The human MCU-EMRE fusion construct with a C-terminal 1D4 tag (TETSQVAPA) was cloned into a pOX vector (Jegla and Salkoff, 1997). Site-directed mutagenesis was performed using the QuickChange kit (Agilent) with mutations verified by sequencing. For in vitro transcription, the pOX vector was first digested with NotI, and then 1 µg of the linearized vector was used for complementary RNA (cRNA) synthesis using the mMessage mMachine T3 transcription kit (Thermo Fisher Scientific) following the manufacturer's instructions. cRNA was purified using the RNeasy MinElute Cleanup kit (Qiagen), dissolved in nuclease-free water to a final concentration of ∼1 µg/µl, and then stored at −80°C. The quality of cRNA was assessed by electrophoresis on denaturing agarose gels containing 4% formaldehyde. The full amino acid sequence of the human MCU-EMRE fusion construct was as follows: MAQNLEGEWQNLGAVYCSTVVPSDDVTVVYQNG LPVISVRLPSRRERCQFTLKPISDSVGVFLRQLQEEDRGIDRVAI YSPDGVRVAASTGIDLLLLDDFKLVINDLTYHVRPPKRDLLSHEN AATLNDVKTLVQQLYTTLCIEQHQLNKERELIERLEDLKEQLAPL EKVRIEISRKAEKRTTLVLWGGLAYMATQFGILARLTWWEYSWDI MEPVTYFITYGSAMAMYAYFVMTRQEYVYPEARDRQYLLFFH KGAKKSRFDLEKYNQLKDAIAQAEMDLKRLRDPLQVHLPLRQ IGEKDVSAAWSGSGRSLVPSRSVIVTRSGAILPKPVKMSFGLLRV FSIVIPFLYVGTLISKNFAALLEEHDIFVPEDDDDDDTETSQVAPA.

Reagents

Ru360 was synthesized in house following a published protocol (Ying et al., 1991; Matlib et al., 1998), with concentrations determined using 360-nm absorption (extinction coefficient, 2.6 × 10^4 M^{-1} cm^{-1}). Other reagents were obtained commercially at the highest grade available.

Handling of *Xenopus* oocytes

Xenopus laevis oocytes were purchased from Nasco and defolliculated by digestion with 1.25 mg/ml type II collagenase (Sigma-Aldrich) at room temperature for 2 h in a solution containing 96 mM NaCl, 2 mM KCl, 2.5 mM $MgCl_2$, 5 mM HEPES, and NaOH, pH 7.4. Stage V–VI oocytes were selected, incubated in 18°C in a ND96 solution (96 mM NaCl, 2 mM KCl, 2 mM $CaCl_2$, 0.5 mM $MgCl_2$, 5 mM HEPES, and NaOH, pH 7.4), and were injected with 50 nl (12–40 ng for TEVC and 40–60 ng for patch clamp) of cRNA using a Nanojet II microinjector (Drummond). Electrophysiological experiments were performed 3–4 d after cRNA injection. During the revision of this paper, we received several batches of oocytes that exhibit low expression of uniporter proteins. The reason is unknown, but it has been reported previously that oocytes could exhibit some seasonal variations in quality. We note that most experiments here were performed in summer and autumn, whereas the revision was in spring.

Oocyte membrane preparations and Western blots

Xenopus oocyte plasma membranes were purified following a published protocol (Wall and Patel, 1989; Kamsteeg and Deen, 2001). In brief, 25 oocytes were homogenized using a Dounce homogenizer in 1.2-ml ice-cold homogenization buffer (HB; 20 mM Tris, 5 mM $MgCl_2$, 5 mM NaH_2PO_4, 1 mM EDTA, and 80 mM sucrose) supplemented with a protease inhibitor cocktail (Roche), and centrifuged for 30 s at 13.5 *g* at 4°C. Then, 1 ml of the top of the sample was removed, and 1 ml HB was added. This step was repeated four times, with centrifugation changed from twice at 13.5 *g* to once at 24 *g* and then to once at 38 *g*. After the last centrifugation, the supernatant was removed. Plasma membranes were spun down for 20 min at 14,000 *g* at 4°C, and then resuspended in 50 µl HB for Western analysis.

Plasma membrane samples were loaded onto 4–20% gels for electrophoresis, and were then transferred to low-fluorescence polyvinylidene difluoride membranes (LI-COR) using a Trans-Blot Turbo transfer system (Bio-Rad). Membranes were blocked in LI-COR Odyssey blocking buffer for 30 min and incubated overnight with an anti-1D4 primary antibody (50 ng/ml, produced in house) in 10 ml TBST (150 mM NaCl, 50 mM Tris, 0.05% Tween-20, and HCl, pH 7.5), and then with a goat anti–mouse IRDye 680RD secondary antibody (1:15,000 in TBST; LI-COR) for 1 h. Western images were acquired using a LI-COR Odyssey CLx imager, and were analyzed with the associated Image Studio software (LI-COR).

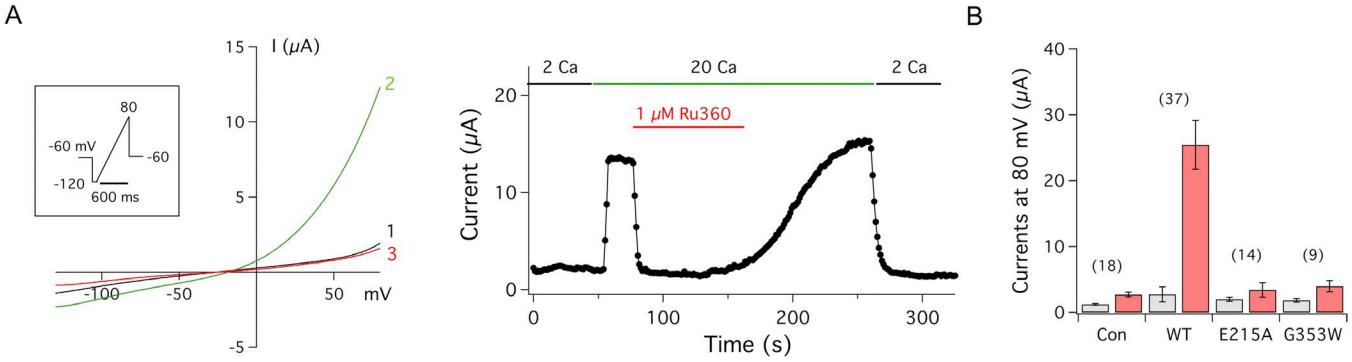

Figure 3. **Uniporter-induced I_{CACC}. (A)** TEVC recordings of hME-expressing oocytes. Currents were recorded using repeated voltage ramps (inset). Left: I–V relations. (1) 2 mM Ca^{2+}. (2) 20 mM Ca^{2+}. (3) 20 mM Ca^{2+} + 1 μM Ru360. Right: Currents at 80 mV. **(B)** I_{CACC} in hME-expressing or uninjected (con) oocytes. The bar chart compares currents (80 mV) induced by 2 mM (gray) and 20 mM (red) extracellular Ca^{2+}. Numbers indicate independent repeats. Data are presented as mean ± SEM.

Electrophysiology

TEVC signals were measured using an Oocyte Clamp OC-725B system (Warner), filtered at 1 kHz, and sampled at 2 kHz. Voltage and current electrodes were pulled and filled with 3 M KCl to have a resistance of 0.5–1.5 MΩ. Data acquisition and membrane voltage control were performed with a pCLAMP-10/Digidata-1322A system (Axon). In all experiments, membrane potentials were held at −60 mV, and repeated voltage ramps were applied as described in the text to allow detection of both uniporter currents and Ca^{2+}-activated Cl^- currents. Oocytes were continuously superfused with the ND96 solution during recordings. In experiments testing dose dependence of currents or divalent-cation conductivity, MCl_2 (M = Ca^{2+}, Sr^{2+}, Mn^{2+}, Ba^{2+}, or Mg^{2+}) and NaCl were varied in pairs as 2 and 96, 5 and 90, 10 and 85, 20 and 70, and 50 and 25 to maintain osmolarities. For experiments requiring intracellular Ca^{2+} chelators, oocytes were injected with 50 nl 0.1-M EGTA (buffered with 10 mM HEPES and NMG, pH 7.4), and then incubated in ND96 supplemented with 100 nM Ru360 for 10–20 min before TEVC. For recordings requiring zero external Cl^-, all anions were substituted with isethionate or gluconate.

Patch clamp recordings were performed using an Axopatch 200B amplifier, interfaced with pCLAMP-10/Digidata-1440A (Axon), with signals filtered at 1 kHz and captured at 5 kHz. Electrodes were filled with 90 mM sodium gluconate, 10 mM NaCl, 5 mM EGTA, 5 mM EDTA, 20 HEPES, and NaOH, pH 7.6, with a pipette resistance of 5–8 MΩ. Oocytes were superfused in ND96 for the formation of gigaohm seals. After obtaining outside-out patches, the bath solution was changed to 100 mM $CaCl_2$, 20 HEPES, and NaOH, pH 7.6 for recording Ca^{2+} currents.

All recordings were performed at room temperature. Negative (inward) currents are defined as currents flowing from the bath to the oocyte cytoplasm (or the cytoplasmic side of outside-out membranes), with bath defined as zero voltage. Raw patch clamp traces were digitally filtered at 50 Hz using the Clampfit software. Data plotting was performed using Igor Pro 7 (WaveMetrics).

Statistics

Data are presented as mean ± SEM. All experiments were repeated at least three times.

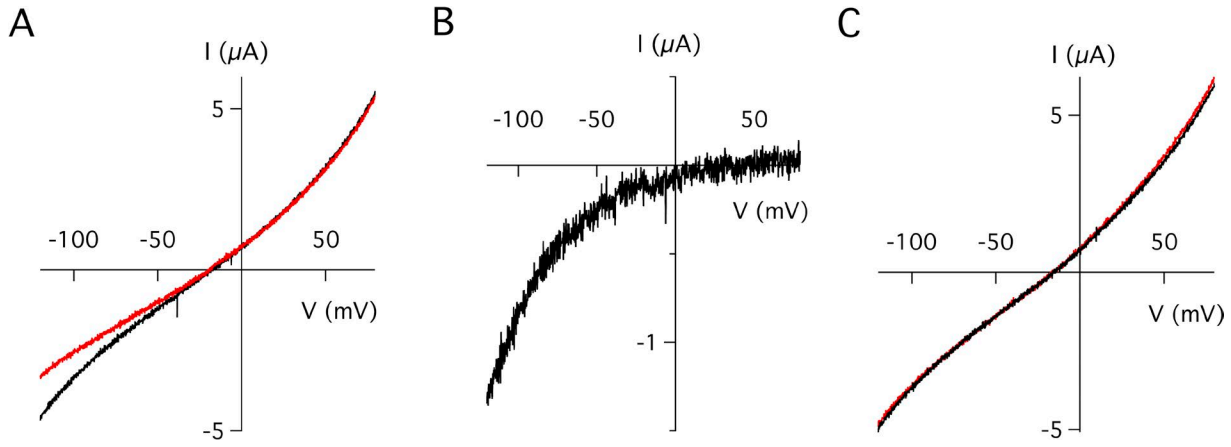

Figure 4. **Isolation of I_{MCU} by applying intracellular Ca^{2+} chelators. (A)** Currents induced by 20 mM extracellular Ca^{2+} in the presence (red) or absence (black) of 1 μM Ru360. Oocytes were preinjected with 5 nmol EGTA and were constantly exposed to 0.5 mM niflumic acid during recordings. **(B)** I_{MCU}, obtained by subtracting Ru360-insentive currents (red in A) from total currents (black in A). **(C)** Currents in uninjected control. Adding Ru360 (red trace) does not affect currents. All traces were digitally filtered at 100 Hz.

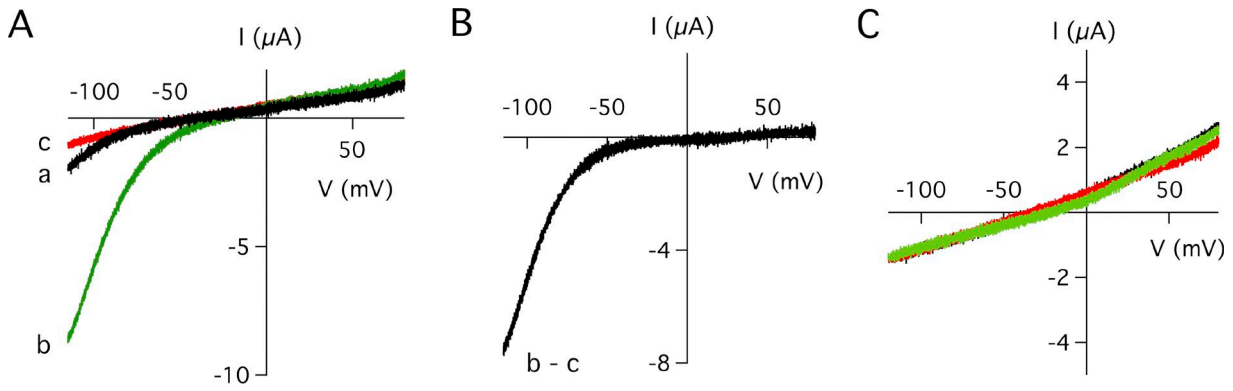

Figure 5. **I_{MCU} in low I_{CACC} oocytes. (A)** Currents induced by: a, 2 mM Ca^{2+}; b, 20 mM Ca^{2+}; and c, 20 mM Ca^{2+} + 1 µM Ru360. **(B)** I_{MCU}, obtained by subtracting c from b. **(C)** Currents from oocytes expressing G353W-hME. Color code is the same as in A.

Online supplemental material

Two supplemental figures are available describing the response of whole-cell currents to niflumic acid (Fig. S1), and documenting uniporter currents recorded in low Cl^- environments (Fig. S2).

Results

The mitoplast patch clamp technique is difficult because it requires the challenging maneuver of obtaining gigaohm-seal patches in small mitochondrial membranes. Our strategy to circumvent this problem is to express the uniporter's TM region, containing MCU and EMRE subunits, in plasma membranes for straightforward electrical recordings. To ensure codelivery of both MCU and EMRE to an alternative membrane system, we used a fully functional tandem construct with human EMRE fused to the C terminus of human MCU (Tsai et al., 2016; hME, Fig. 1). This construct was initially expressed in HEK 293 cells, but despite multiple attempts in varying cell culture conditions and protein engineering (i.e., deleting the mitochondrial targeting sequence and/or including an N-terminal glycophorin-A sequence), no plasma-membrane expression was detected using immunostaining of fixed cells.

We thus turned to *Xenopus* oocyte expression, a classical system for ion channel electrophysiology. Injecting 12 ng cRNA of mitochondrial targeting sequence–truncated hME (hereafter defined as WT hME, sequence available in Materials and methods) into oocytes led to expression of a full-length 45-kD protein in purified plasma membranes after 3–4 d of incubation (Fig. 2). TEVC analysis using repeated voltage ramps from –120 to 80 mV shows that increasing external Ca^{2+} from 2 to 20 mM induces large Ca^{2+}-activated Cl^- currents (I_{CACC}; Hartzell, 1996; Yao and Tsien, 1997), which exhibit a diagnostic outwardly rectifying I–V relation (Fig. 3 A), a reversal potential of –25 mV near the Cl^- equilibrium potential (Fig. 3 A), and strong responses to an I_{CACC} inhibitor niflumic acid (NFA; White and Aylwin, 1990; Fig. S1). This I_{CACC} is induced by Ca^{2+} influx via the uniporter (I_{MCU}), as it is inhibited by Ru360 (Fig. 3 A), and is ∼10-fold smaller in uninjected controls or in oocytes expressing nonfunctional mutants E215A (E264A in MCU; Baughman et al., 2011) and G353W (G81W in EMRE; Tsai et al., 2016; Fig. 2 and 3 B).

The existence of large I_{CACC} poses a problem for our analysis: Ru360-sensitive currents would contain both I_{MCU} and I_{CACC} (Fig. 3 A), thus making it impossible to specifically characterize I_{MCU}. To overcome this problem, we applied NFA along with

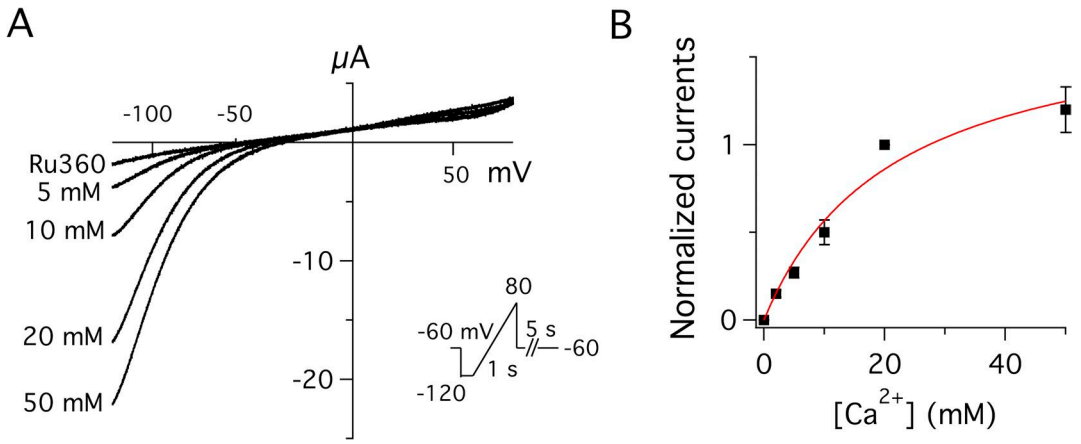

Figure 6. **Ca^{2+} dose response of I_{MCU}. (A)** I–V curves of I_{MCU} in various external [Ca^{2+}]. **(B)** A dose–response plot. Currents (measured at –120 mV) induced by 2, 5, 10, and 50 mM Ca^{2+} were normalized to currents induced by 20 mM Ca^{2+}. A Michaelis-Menten equation was used for data fit (red curve). Each data point represents five to eight repeats. Data are presented as mean ± SEM.

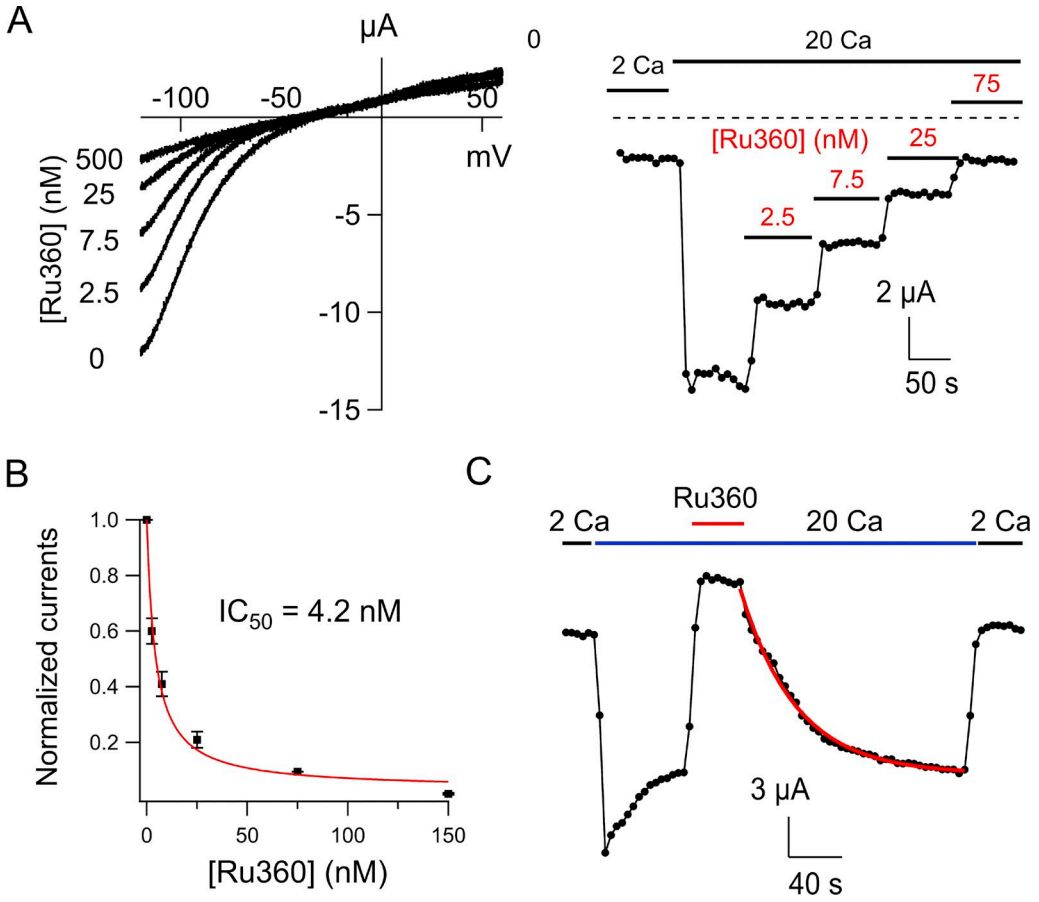

Figure 7. **Ru360 inhibition of I_{MCU}. (A)** Left: I–V relation of I_{MCU} in the presence of 20 mM Ca^{2+} and various concentrations of Ru360. Right: currents at −120 mV plotted in a time course. **(B)** A Ru360 dose-response curve. Data fitting uses a standard single-site binding model (red curve). Each data point represents the mean of at least five independent repeats. Data are presented as mean ± SEM. **(C)** Current (−120 mV) recovery upon Ru360 (500 nM) removal follows a single exponential curve (red). The voltage protocol is the same as in Fig. 6.

intracellular Ca^{2+} chelators (5 nmol EGTA) to inhibit I_{CACC}, as has been done previously to unmask endogenous store-operated Ca^{2+} currents (Hartzell, 1996; Yao and Tsien, 1997). Under this condition, 20 mM Ca^{2+} elicits Ru360-sensitive I_{MCU} with an amplitude of 0.5–2 μA at −120 mV, exhibiting an inwardly rectifying I–V relation that plateaus near zero current (Fig. 4, A and B), closely resembling uniporter currents observed in the mitoplast patch clamp. In contrast, adding Ru360 fails to affect currents recorded in control cells with no hME expression (Fig. 4 C). As an alternative means to suppress I_{CACC}, we soaked oocytes in a Cl^--free condition for 3 d to remove 80% of intracellular Cl^- (Fig. S2), and then performed TEVC recordings in a Cl^--free extracellular medium supplied with NFA. Currents induced by 20 mM Ca^{2+} rectify inwardly (Fig. S2), similar to observations made with oocytes containing intracellular EGTA (Fig. 4 B).

Our attempts to enhance uniporter currents by injecting more cRNA (30–40 ng) lead to enormous Ca^{2+}-induced, outwardly rectifying I_{CACC} approaching 100 μA at 80 mV in most oocytes. Surprisingly, in a subset of oocytes (ranging from 5–30% in six independent batches), Ca^{2+}-activated Cl^- channels appear to be inactivated: outward currents are small (1–5 μA) and are unaffected by increasing external Ca^{2+} or adding Ru360 (Fig. 5 A). Moreover, the I–V curve is little affected by adding NFA (Fig. S1). The mechanism underlying this Ca^{2+}-activated Cl^- channel down-regulation is unclear, but similar phenomena have been reported before when foreign proteins were expressed in *Xenopus* oocytes (Jorgensen et al., 1997; Kunzelmann et al., 1997). With I_{CACC} inactivated, I_{MCU} can now be isolated without EGTA injection (Fig. 4 B) or extensive Cl^- dialysis (Fig. S2), maneuvers that often make oocyte membranes unstable. Control experiments show that I_{MCU} is absent in cells expressing nonfunctional E215A or G353W mutants (Fig. 5 C). In TEVC experiments below, these low-I_{CACC} oocytes were used to further characterize uniporter properties.

We first titrated Ca^{2+} to obtain the dose response of I_{MCU}, yielding a K_m of 22 mM (Fig. 6). Increasing Ru360 concentration in the presence of 20 mM Ca^{2+} progressively inhibits the uniporter with a half maximal inhibitory concentration (IC_{50}) of 4.2 nM (Fig. 7, A and B). Recovery of Ca^{2+} currents after Ru360 withdrawal follows a slow time course with a time constant of 28 ± 5 s (Fig. 7 C). I_{MCU} shows a divalent cation conductivity of $Ca^{2+} > Sr^{2+} >> Ba^{2+}$, Mn^{2+}, and Mg^{2+} (Fig. 8). In the presence of 10 mM Ca^{2+}, I_{MCU} is inhibited by Mn^{2+} with an IC_{50} of 410 μM (Fig. 9, A and B). It is also slightly reduced by 9 ± 3% by 10 mM Mg^{2+} (unpublished data), a result consistent with experiments using mitochondrial Ca^{2+} uptake (Bragadin et al., 1979) or mitoplast patch clamp (Kirichok et al., 2004).

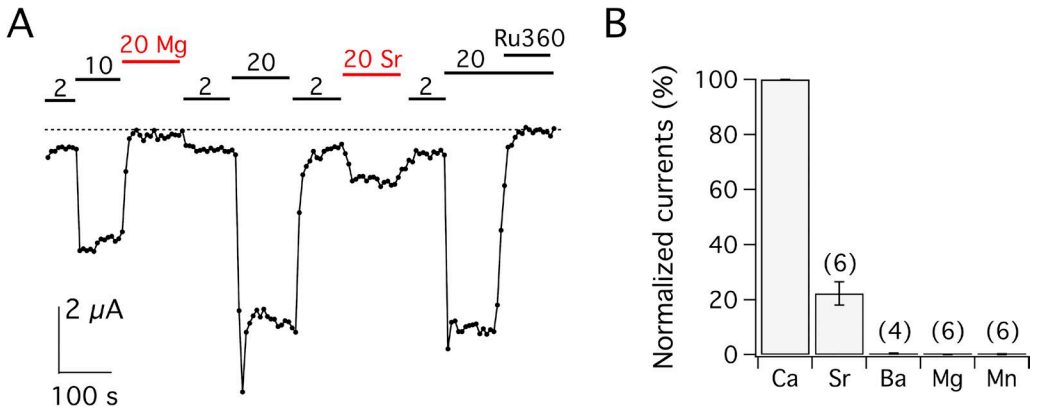

Figure 8. **Divalent cation conductivity. (A)** Currents (−120 mV) of hME elicited by 20 mM of various divalent cations. Black bars indicate Ca^{2+} concentrations in mM. The voltage protocol is the same as in Fig. 6. **(B)** A comparison of divalent cation transport. All currents were induced by 20 mM divalent cations. Data are presented as mean ± SEM.

Although TEVC is highly efficient in measuring whole-cell currents, it has certain limitations, including difficulties in controlling intracellular solutions and incompatibility with single-channel recordings. To circumvent these problems, we used the patch clamp to record hME in excised outside-out patches. In these experiments, 5 mM EGTA and EDTA were added to the pipette solution to eliminate I_{CACC}, and 100 mM $CaCl_2$ was placed in the bath to elicit I_{MCU}. Of 45 patches tested, 4 exhibited macroscopic Ca^{2+} currents of >5 pA strongly inhibited by extracellularly applied Ru360 (200 nM), with removal of Ru360 yielding an unblock time constant of 17 ± 4 s (Fig. 10, A and B), in good agreement with the kinetics seen in TEVC. Moreover, 11 patches showed Ru360-sensitive currents of 1–5 pA, allowing observation of single-channel openings (Fig. 10, C and D). At a holding membrane potential of −80 mV, the uniporter has a single-channel amplitude of ∼0.3 pA. Ru360 does not affect the current amplitude, but greatly shortens the channel open time. None of these electrical phenomena were observed in 30 outside-out patches excised from uninjected oocytes or in 15 patches from oocytes expressing the G353W mutant. Altogether, these results demonstrate the suitability of the *Xenopus* oocyte system for more extensive patch clamp analysis of the uniporter in the future.

Discussion

In the current study, we expressed the Ca^{2+}-conducting TM region of the human uniporter in the form of an MCU-EMRE fusion construct in *Xenopus* oocyte plasma membranes. TEVC and patch clamp recordings show that these proteins produce $I_{MCU,}$ which is fully inhibited by Ru360 from the extracellular side. As Ru360 is known to block MCU from the mitochondrial IMS (Cao et al., 2017), we infer that hME adopts a homogeneous IMS-side-out orientation in oocyte membranes. Further characterization of I_{MCU} reveals a Ca^{2+} dose response, I–V relation, single-channel amplitude, and divalent cation selectivity remarkably similar to observations made using the mitoplast patch clamp (Kirichok et al., 2004; Table 1). In addition, inhibition of I_{MCU} by Mn^{2+} is a feature commonly seen in other Ca^{2+}-selective channels (Sather and McCleskey, 2003). Finally, I_{MCU} is fully

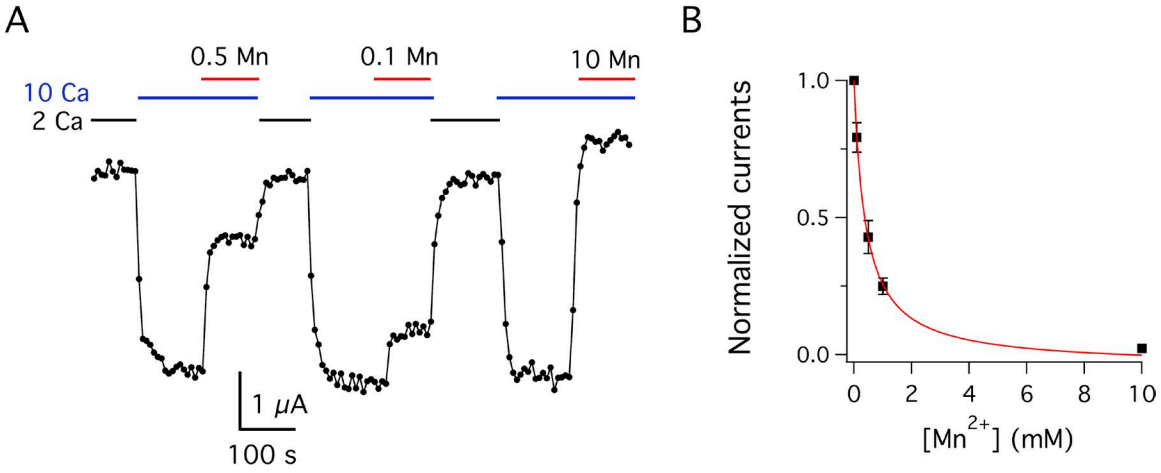

Figure 9. **Mn^{2+} inhibition of I_{MCU}. (A)** Inhibition of I_{MCU} (−120 mV) by Mn^{2+} at indicated concentrations in mM. **(B)** A dose response of Mn^{2+} inhibition. Curve fitting (red curve) assumes single-site binding. Data are presented as mean ± SEM.

Table 1. **Comparison of uniporter properties characterized using mitoplast patch clamp or *Xenopus* oocyte recordings**

Methods	Mitoplast patch clamp	*Xenopus* oocyte recordings
Half activating [Ca^{2+}]	19 mM	22 mM
Ru360 IC_{50}	1.7 nM	4.2 nM
Divalent ion selectivity	Ca^{2+} ~ Sr^{2+} >> Mn^{2+} ~ Ba^{2+} >> Mg^{2+}	Ca^{2+} > Sr^{2+} >> Mn^{2+}, Ba^{2+}, and Mg^{2+}
Single-channel amplitude (−80 mV)	<0.5 pA (symmetrical 105 mM Ca^{2+})	~0.3 pA (100 mM extracellular Ca^{2+} and <1 nM cytoplasmic Ca^{2+})

abolished by mutations known to eliminate uniporter function in mitochondria: E215A (E264A in MCU), which destroys a Ca^{2+} site in the MCU pore (Baughman et al., 2011; Cao et al., 2017), and G353W (G81W in EMRE), which disrupts TM interactions between MCU and EMRE (Tsai et al., 2016). Collectively, these results unambiguously rule out electrical artifacts, and demonstrate that the human uniporter exhibits similar ion-conducting behaviors in mitochondrial and *Xenopus* oocyte membranes.

Three issues about our method are discussed here. First, we refrained from using the most well-known inhibitor of the

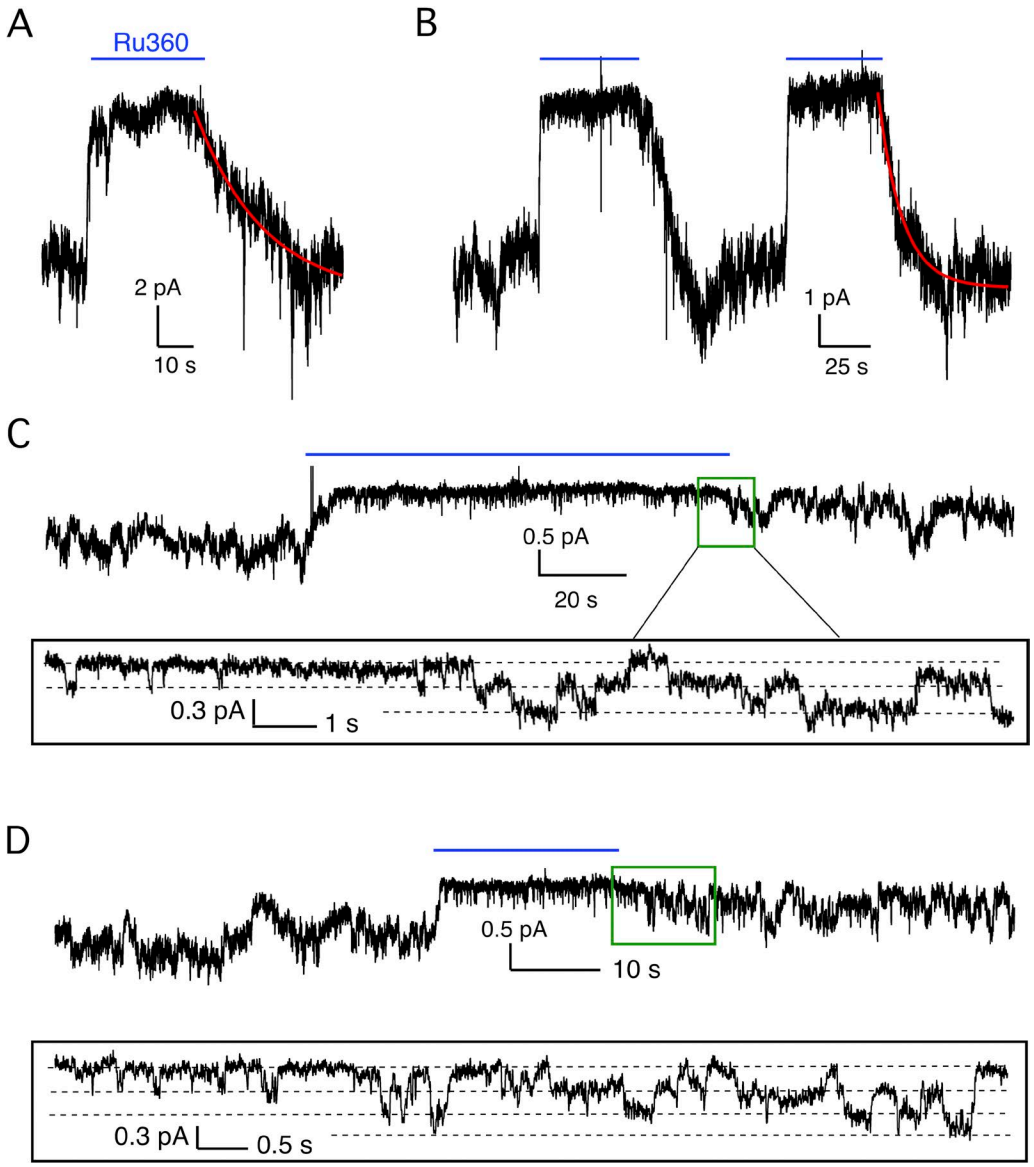

Figure 10. **Patch clamp outside-out recordings of hME. (A and B)** Macroscopic recordings with currents >5 pA. **(C and D)** Recordings with discernible single-channel events. Red curves: Single exponential fit of current recovery after Ru360 removal. Blue bars: 200 nM Ru360. Bath contains 100 mM Ca^{2+}. Pipette solutions contain 5 mM EGTA and 5 mM EDTA to reduce free Ca^{2+} below 1 nM to inhibit I_{CACC}. Voltage was clamped at −80 mV for all recordings.

uniporter, ruthenium red (Rigoni and Deana, 1986), as this hexavalent compound can nonspecifically inhibit several Ca^{2+} transport proteins, such as ryanodine receptors (Ma, 1993) and voltage-gated Ca^{2+} channels (Cibulsky and Sather, 1999). Ru360 is a divalent ruthenium amine complex that specifically and potently inhibits the uniporter (Ying et al., 1991; Matlib et al., 1998). Second, the use of a tandem hME construct neither assumes nor implies an MCU-EMRE interacting stoichiometry of 1:1—the number of EMRE subunits associated with MCU is currently unknown. The purpose of using this construct is to ensure that both MCU and EMRE travel to the plasma membrane to assemble into a functional channel. We cannot perform recordings by coinjecting MCU and EMRE cRNAs into oocytes, as MCU fails to travel to plasma membranes without EMRE fused to its C terminus. Third, the regulatory MICU subunits are entirely omitted in this study. It might seem plausible to incubate purified MICU proteins with *Xenopus* oocytes to form a full uniporter complex, but we were reluctant to do so because the oligomerization status of MICUs is the subject of current uncertainty: these subunits have been shown to form homodimers (Wang et al., 2014; Li et al., 2016; Kamer et al., 2017), homohexamers (Wang et al., 2014), and heterodimers with or without an intersubunit disulfide (Patron et al., 2014; Petrungaro et al., 2015; Kamer et al., 2017). It is unclear which of these can properly assemble with the Ca^{2+}-conducting subunits to gate the uniporter. Adding MICUs to our electrical analysis would be premature before these conflicts are resolved.

In the last few years, there have been reports describing single-channel recordings of the uniporter using reconstituted planar lipid bilayers (De Stefani et al., 2011; Patron et al., 2014; Wu et al., 2018). These recordings are problematic for several reasons. First, size-exclusion chromatography has not been used to test if uniporter proteins are denatured during detergent solubilization, a very common issue in membrane-protein purification. Second, macroscopic recordings have not been reported in these studies, making it difficult to judge if observed single channels exhibit representative uniporter behaviors. This raises serious concerns as electrical properties described in these reports are vastly different from those obtained using the mitoplast patch clamp (Kirichok et al., 2004). Third, none of these recordings show reversible block by ruthenium red or Ru360. In our hands, ruthenium compounds can occasionally perturb planar bilayers, leading to irreversible loss of channel activities.

Results here also have implications in two controversies in the field. First, the TM orientation of EMRE is currently in dispute regarding whether the N terminus of this single-pass IMM protein faces IMS or the matrix (Tsai et al., 2016; Vais et al., 2016; Yamamoto et al., 2016). That the hME construct can form functional channels is a powerful demonstration that EMRE's N terminus is located in the matrix where MCU's C-terminal region also resides. Second, based on electrical recordings in reconstituted bilayers, it was proposed that human MCU by itself is sufficient to conduct Ca^{2+} (De Stefani et al., 2011; Patron et al., 2014). This argument has been undermined by mitochondrial assays showing that EMRE is also required for uniporter-mediated mitochondrial Ca^{2+} uptake (Sancak et al., 2013; Kovács-Bogdán et al., 2014; Tsai et al., 2016), and is unambiguously rejected here with recordings showing that the G353W mutation eliminates Ca^{2+} currents of hME (Fig. 5 C).

In summary, we have established an efficient *Xenopus* oocyte system to record electrical behaviors of the human uniporter. This achievement now permits quantitative work in the future using TEVC or patch clamp electrophysiology to shed light on fundamental mechanisms underlying the crucial roles of the uniporter in mammalian pathophysiology.

Acknowledgments

We thank Dr. Willem Laursen and Dr. Gonzalo Budelli for technical assistance with TEVC, and Dr. Paul Garrity and Dr. David Clapham for lending us some electrophysiological equipment. We particularly thank Dr. Christopher Miller for constructive suggestions and unconditional support during the development of this project.

C.-W. Tsai is supported by National Institutes of Health grant R01-GM-107023.

The authors declare no competing financial interests.

Author contributions: Both C.-W. Tsai and M.-F. Tsai performed experiments and analyzed data. C.-W. Tsai prepared the figures, and M.-F. Tsai wrote the manuscript.

Richard W. Aldrich served as editor.

Submitted: 29 January 2018
Accepted: 22 May 2018

References

Baughman, J.M., F. Perocchi, H.S. Girgis, M. Plovanich, C.A. Belcher-Timme, Y. Sancak, X.R. Bao, L. Strittmatter, O. Goldberger, R.L. Bogorad, et al. 2011. Integrative genomics identifies MCU as an essential component of the mitochondrial calcium uniporter. *Nature.* 476:341–345. https://doi.org/10.1038/nature10234

Bernardi, P. 1999. Mitochondrial transport of cations: channels, exchangers, and permeability transition. *Physiol. Rev.* 79:1127–1155. https://doi.org/10.1152/physrev.1999.79.4.1127

Bragadin, M., T. Pozzan, and G.F. Azzone. 1979. Kinetics of Ca2+ carrier in rat liver mitochondria. *Biochemistry.* 18:5972–5978. https://doi.org/10.1021/bi00593a033

Cao, C., S. Wang, T. Cui, X.C. Su, and J.J. Chou. 2017. Ion and inhibitor binding of the double-ring ion selectivity filter of the mitochondrial calcium uniporter. *Proc. Natl. Acad. Sci. USA.* 114:E2846–E2851. https://doi.org/10.1073/pnas.1620316114

Cibulsky, S.M., and W.A. Sather. 1999. Block by ruthenium red of cloned neuronal voltage-gated calcium channels. *J. Pharmacol. Exp. Ther.* 289:1447–1453.

Csordás, G., T. Golenár, E.L. Seifert, K.J. Kamer, Y. Sancak, F. Perocchi, C. Moffat, D. Weaver, S. de la Fuente Perez, R. Bogorad, et al. 2013. MICU1 controls both the threshold and cooperative activation of the mitochondrial Ca^{2+} uniporter. *Cell Metab.* 17:976–987. https://doi.org/10.1016/j.cmet.2013.04.020

De Stefani, D., A. Raffaello, E. Teardo, I. Szabò, and R. Rizzuto. 2011. A forty-kilodalton protein of the inner membrane is the mitochondrial calcium uniporter. *Nature.* 476:336–340. https://doi.org/10.1038/nature10230

Gunter, T.E., L. Buntinas, G. Sparagna, R. Eliseev, and K. Gunter. 2000. Mitochondrial calcium transport: mechanisms and functions. *Cell Calcium.* 28:285–296. https://doi.org/10.1054/ceca.2000.0168

Hartzell, H.C. 1996. Activation of different Cl currents in *Xenopus* oocytes by Ca liberated from stores and by capacitative Ca influx. *J. Gen. Physiol.* 108:157–175. https://doi.org/10.1085/jgp.108.3.157

Jegla, T., and L. Salkoff. 1997. A novel subunit for shal K+ channels radically alters activation and inactivation. *J. Neurosci.* 17:32–44. https://doi.org/10.1523/JNEUROSCI.17-01-00032.1997

Jorgensen, A.J., P. Bennekou, K. Eskesen, and B.I. Kristensen. 1997. Annexins from Ehrlich ascites cells inhibit the calcium-activated chloride current in Xenopus laevis oocytes. *Pflugers Arch.* 434:261–266. https://doi.org/10.1007/s004240050394

Kamer, K.J., and V.K. Mootha. 2015. The molecular era of the mitochondrial calcium uniporter. *Nat. Rev. Mol. Cell Biol.* 16:545–553. https://doi.org/10.1038/nrm4039

Kamer, K.J., Z. Grabarek, and V.K. Mootha. 2017. High-affinity cooperative Ca^{2+} binding by MICU1-MICU2 serves as an on-off switch for the uniporter. *EMBO Rep.* 18:1397–1411. https://doi.org/10.15252/embr.201643748

Kamsteeg, E.J., and P.M. Deen. 2001. Detection of aquaporin-2 in the plasma membranes of oocytes: a novel isolation method with improved yield and purity. *Biochem. Biophys. Res. Commun.* 282:683–690. https://doi.org/10.1006/bbrc.2001.4629

Kirichok, Y., G. Krapivinsky, and D.E. Clapham. 2004. The mitochondrial calcium uniporter is a highly selective ion channel. *Nature.* 427:360–364. https://doi.org/10.1038/nature02246

Kovács-Bogdán, E., Y. Sancak, K.J. Kamer, M. Plovanich, A. Jambhekar, R.J. Huber, M.A. Myre, M.D. Blower, and V.K. Mootha. 2014. Reconstitution of the mitochondrial calcium uniporter in yeast. *Proc. Natl. Acad. Sci. USA.* 111:8985–8990. https://doi.org/10.1073/pnas.1400514111

Kunzelmann, K., M. Mall, M. Briel, A. Hipper, R. Nitschke, S. Ricken, and R. Greger. 1997. The cystic fibrosis transmembrane conductance regulator attenuates the endogenous Ca2+ activated Cl- conductance of Xenopus oocytes. *Pflugers Arch.* 435:178–181. https://doi.org/10.1007/s004240050498

Kwong, J.Q., X. Lu, R.N. Correll, J.A. Schwanekamp, R.J. Vagnozzi, M.A. Sargent, A.J. York, J. Zhang, D.M. Bers, and J.D. Molkentin. 2015. The Mitochondrial Calcium Uniporter Selectively Matches Metabolic Output to Acute Contractile Stress in the Heart. *Cell Reports.* 12:15–22. https://doi.org/10.1016/j.celrep.2015.06.002

Li, D., W. Wu, H. Pei, Q. Wei, Q. Yang, J. Zheng, and Z. Jia. 2016. Expression and preliminary characterization of human MICU2. *Biol. Open.* 5:962–969. https://doi.org/10.1242/bio.018572

Liu, J.C., J. Liu, K.M. Holmström, S. Menazza, R.J. Parks, M.M. Fergusson, Z.X. Yu, D.A. Springer, C. Halsey, C. Liu, et al. 2016. MICU1 Serves as a Molecular Gatekeeper to Prevent In Vivo Mitochondrial Calcium Overload. *Cell Reports.* 16:1561–1573. https://doi.org/10.1016/j.celrep.2016.07.011

Logan, C.V., G. Szabadkai, J.A. Sharpe, D.A. Parry, S. Torelli, A.M. Childs, M. Kriek, R. Phadke, C.A. Johnson, N.Y. Roberts, et al. UK10K Consortium. 2014. Loss-of-function mutations in MICU1 cause a brain and muscle disorder linked to primary alterations in mitochondrial calcium signaling. *Nat. Genet.* 46:188–193. https://doi.org/10.1038/ng.2851

Luongo, T.S., J.P. Lambert, A. Yuan, X. Zhang, P. Gross, J. Song, S. Shanmughapriya, E. Gao, M. Jain, S.R. Houser, et al. 2015. The Mitochondrial Calcium Uniporter Matches Energetic Supply with Cardiac Workload during Stress and Modulates Permeability Transition. *Cell Reports.* 12:23–34. https://doi.org/10.1016/j.celrep.2015.06.017

Ma, J. 1993. Block by ruthenium red of the ryanodine-activated calcium release channel of skeletal muscle. *J. Gen. Physiol.* 102:1031–1056. https://doi.org/10.1085/jgp.102.6.1031

Mallilankaraman, K., P. Doonan, C. Cárdenas, H.C. Chandramoorthy, M. Müller, R. Miller, N.E. Hoffman, R.K. Gandhirajan, J. Molgó, M.J. Birnbaum, et al. 2012. MICU1 is an essential gatekeeper for MCU-mediated mitochondrial Ca(2+) uptake that regulates cell survival. *Cell.* 151:630–644. https://doi.org/10.1016/j.cell.2012.10.011

Matlib, M.A., Z. Zhou, S. Knight, S. Ahmed, K.M. Choi, J. Krause-Bauer, R. Phillips, R. Altschuld, Y. Katsube, N. Sperelakis, and D.M. Bers. 1998. Oxygen-bridged dinuclear ruthenium amine complex specifically inhibits Ca2+ uptake into mitochondria in vitro and in situ in single cardiac myocytes. *J. Biol. Chem.* 273:10223–10231. https://doi.org/10.1074/jbc.273.17.10223

Oxenoid, K., Y. Dong, C. Cao, T. Cui, Y. Sancak, A.L. Markhard, Z. Grabarek, L. Kong, Z. Liu, B. Ouyang, et al. 2016. Architecture of the mitochondrial calcium uniporter. *Nature.* 533:269–273. https://doi.org/10.1038/nature17656

Patron, M., V. Checchetto, A. Raffaello, E. Teardo, D. Vecellio Reane, M. Mantoan, V. Granatiero, I. Szabò, D. De Stefani, and R. Rizzuto. 2014. MICU1 and MICU2 finely tune the mitochondrial Ca2+ uniporter by exerting opposite effects on MCU activity. *Mol. Cell.* 53:726–737. https://doi.org/10.1016/j.molcel.2014.01.013

Penna, E., J. Espino, D. De Stefani, and R. Rizzuto. 2018. The MCU complex in cell death. *Cell Calcium.* 69:73–80.

Petrungaro, C., K.M. Zimmermann, V. Küttner, M. Fischer, J. Dengjel, I. Bogeski, and J. Riemer. 2015. The Ca(2+)-Dependent Release of the Mia40-Induced MICU1-MICU2 Dimer from MCU Regulates Mitochondrial Ca(2+) Uptake. *Cell Metab.* 22:721–733. https://doi.org/10.1016/j.cmet.2015.08.019

Rigoni, F., and R. Deana. 1986. Ruthenium red inhibits the mitochondrial Ca2+ uptake in intact bovine spermatozoa and increases the cytosolic Ca2+ concentration. *FEBS Lett.* 198:103–108. https://doi.org/10.1016/0014-5793(86)81193-0

Rizzuto, R., D. De Stefani, A. Raffaello, and C. Mammucari. 2012. Mitochondria as sensors and regulators of calcium signalling. *Nat. Rev. Mol. Cell Biol.* 13:566–578. https://doi.org/10.1038/nrm3412

Sancak, Y., A.L. Markhard, T. Kitami, E. Kovács-Bogdán, K.J. Kamer, N.D. Udeshi, S.A. Carr, D. Chaudhuri, D.E. Clapham, A.A. Li, et al. 2013. EMRE is an essential component of the mitochondrial calcium uniporter complex. *Science.* 342:1379–1382. https://doi.org/10.1126/science.1242993

Sather, W.A., and E.W. McCleskey. 2003. Permeation and selectivity in calcium channels. *Annu. Rev. Physiol.* 65:133–159. https://doi.org/10.1146/annurev.physiol.65.092101.142345

Tsai, M.F., C.B. Phillips, M. Ranaghan, C.W. Tsai, Y. Wu, C. Willliams, and C. Miller. 2016. Dual functions of a small regulatory subunit in the mitochondrial calcium uniporter complex. *eLife.* 5:e15545. https://doi.org/10.7554/eLife.15545

Vais, H., K. Mallilankaraman, D.D. Mak, H. Hoff, R. Payne, J.E. Tanis, and J.K. Foskett. 2016. EMRE Is a Matrix Ca(2+) Sensor that Governs Gatekeeping of the Mitochondrial Ca(2+) Uniporter. *Cell Reports.* 14:403–410. https://doi.org/10.1016/j.celrep.2015.12.054

Wall, D.A., and S. Patel. 1989. Isolation of plasma membrane complexes from Xenopus oocytes. *J. Membr. Biol.* 107:189–201. https://doi.org/10.1007/BF01871724

Wang, L., X. Yang, S. Li, Z. Wang, Y. Liu, J. Feng, Y. Zhu, and Y. Shen. 2014. Structural and mechanistic insights into MICU1 regulation of mitochondrial calcium uptake. *EMBO J.* 33:594–604. https://doi.org/10.1002/embj.201386523

White, M.M., and M. Aylwin. 1990. Niflumic and flufenamic acids are potent reversible blockers of Ca2(+)-activated Cl- channels in Xenopus oocytes. *Mol. Pharmacol.* 37:720–724.

Wu, G., S. Li, G. Zong, X. Liu, S. Fei, L. Shen, X. Guan, X. Yang, and Y. Shen. 2018. Single channel recording of a mitochondrial calcium uniporter. *Biochem. Biophys. Res. Commun.* 496:127–132. https://doi.org/10.1016/j.bbrc.2018.01.010

Yamamoto, T., R. Yamagoshi, K. Harada, M. Kawano, N. Minami, Y. Ido, K. Kuwahara, A. Fujita, M. Ozono, A. Watanabe, et al. 2016. Analysis of the structure and function of EMRE in a yeast expression system. *Biochim. Biophys. Acta.* 1857:831–839. https://doi.org/10.1016/j.bbabio.2016.03.019

Yao, Y., and R.Y. Tsien. 1997. Calcium current activated by depletion of calcium stores in *Xenopus* oocytes. *J. Gen. Physiol.* 109:703–715. https://doi.org/10.1085/jgp.109.6.703

Ying, W.L., J. Emerson, M.J. Clarke, and D.R. Sanadi. 1991. Inhibition of mitochondrial calcium ion transport by an oxo-bridged dinuclear ruthenium ammine complex. *Biochemistry.* 30:4949–4952. https://doi.org/10.1021/bi00234a016